Proceedings of the Joint Austrian Computer Vision and Robotics Workshop 2020 DOI: 10.3217/978-3-85125-752-6-19

Ground Control Point Retrieval From SAR Satellite Imagery

Roland Perko, Hannes Raggam, Karlheinz Gutjahr
JOANNEUM RESEARCH Forschungsgesellschaft mbH, DIGITAL
{roland.perko,hannes.raggam,karlheinz.gutjahr}@joanneum.at

Wolfgang Koppe, Jürgen Janoth
Airbus Defence and Space
{wolfgang.koppe,juergen.janoth}@airbus.com

Abstract. *For many applications, like for instance autonomous driving or geo-referencing of optical satellite data, highly accurate reference coordinates are of importance. This work demonstrates that such Ground Control Points can automatically be derived from multi-beam Synthetic Aperture Radar satellite images with high accuracy.*

1. Introduction

Reliable Ground Control Points (GCPs), i.e., points of known geographical coordinates, are an essential input for the precise ortho-rectification of remote sensing imagery, the exact location of targets or the accurate geo-referencing of a variety of geo-datasets. Although GCPs collected by terrestrial means typically offer a high accuracy, their acquisition is expensive especially on a worldwide level.

Thus, a concept was formed to extract such GCPs from Synthetic Aperture Radar (SAR) satellite images (e.g., [9, 11]). Recently, refined SAR-based GCP extraction emerged due to three main reasons: (1) The 2D geo-location accuracy of current SAR sensors is very high, actually at centimeter level if atmospheric effects and Earth surface displacements are taken into account [5]. (2) Metallic objects like lamp poles or traffic signs (i.e., common features in urban scenes) appear as focused points in SAR images and can be detected with subpixel accuracy. (3) Using stereo acquisitions the 3D position (actually the ground mark) of these objects can be computed by means of radargrammetry.

Therefore, this work presents an automatic workflow, combining techniques from photogrammetric computer vision and remote sensing, that derives highly accurate GCPs from a set of multi-beam[1] high resolution images from TerraSAR-X, TanDEM-X, or PAZ satellites [3]. In contrast to [11], where persistent scatter interferometry (PSI) is deployed for point detection and 3D reconstruction, we build upon computer vision paradigms. Thus, the presented method can be efficiently applied on single images while PSI needs a stack of multiple images and is computationally very demanding [4]. In addition, our method can be applied on amplitude images alone as it does not rely on the phase information of the signal.

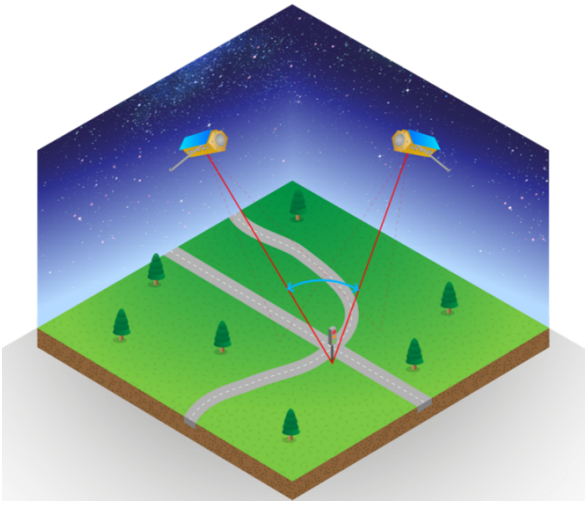

Figure 1. Stereo acquisition from space. Shown are two SAR satellites observing the same region on ground from two different orbital directions and look angles.

2. Method

The proposed fully automatic workflow for GCP retrieval consists of the following steps:

[1]The term *multi-beam* is equivalent to what is called *multi-view* in computer vision and stems from digital beamforming.

Image acquisition. Acquisition of a set of SAR images of the area of interest, in optimal case from ascending and descending orbital direction (cf. Figure 1). In case images are gathered from one orbital direction the stereo intersection angle has to be reasonably large (i.e., larger than $10°$). After import each image consists of complex valued pixels plus the according sensor model (i.e., the cocircular geometry based on the Range and Doppler equations [2, 10]).

SAR delay correction. Adjustment of sensor models, in specific the SAR internal delays in range direction, for the following effects (cf. [5]): (1) Ionospheric signal propagation delay caused by electrons; (2) tropospheric signal propagation delay caused by air conditions, e.g., water vapor; (3) solid earth tides caused by gravity of moon and sun; and (4) plate tectonics, i.e., continental drift. For each image the range correction grid is updated, whereas the underlying information is gathered from weather and GPS services.

Point extraction. Metal objects appear as points or rather bright blobs on dark background (cf. Figure 2). For detection the image is upsampled based on complex FFT oversampling with a factor of 2. Then a matched filter is applied on the amplitude to localize blobs using a spike-shaped template kernel (cf. [14]). Results are thresholded and the best matching 2D blob locations are retrieved by subpixel interpolation [6, 12].

Matching of points. For each stereo pair epipolar rectified images using a coarse digital elevation model based on the method [13] are generated, also transferring the extracted points. This method undistorts the images in range direction and thus increases their geometric and radiometric similarity. Those points are then matched by means of normalized cross-correlation (kernel size depends on resolution of the input images). The resulting homologous points are then transformed back into the input images.

Retrieval of 3D coordinates. GCPs are calculated by a multi-image least squares spatial intersection of SAR range circles yielding a point cloud. Due to over determination incorrect points can be detected and rejected.

3. Results and Conclusion

The presented workflow was applied on a multitude of multi-beam scenes distributed over the whole globe, acquired with various imaging modes (i.e., Stripmap, Spotlight, HS Spotlight, Staring Spotlight [3]). Reference coordinates of metal poles were measured in-situ with differential GPS with an absolute 3D accuracy of ± 5 cm such that inaccuracies of the cadastre system do not propagate into the evaluation.

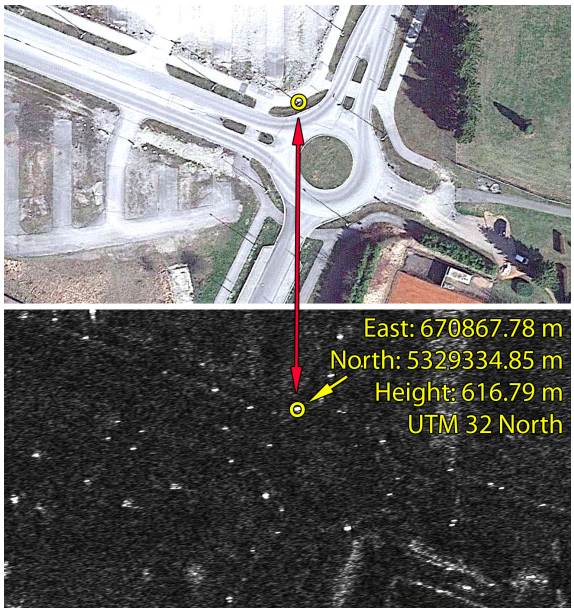

Figure 2. Roundabout traffic as perceived from an airborne digital camera (top) and from the SAR satellite (bottom). The bright blobs in the SAR amplitude corresponds mainly to light poles. An exemplary pole is highlighted together with its extracted 3D location.

Table 1 gives exemplary 3D accuracies (defined as root mean square (rms) values) as can be expected from the proposed methodology. In planimetry around 15 cm are achieved and in height around 20 cm, which are impressive numbers taking into account the altitude of the satellite's orbit at 514 km.

	East [m]	North [m]	Height [m]
rms	0.14	0.14	0.21
mean	0.04	0.09	0.07
std	0.13	0.10	0.20
min	-0.38	-0.26	-0.44
max	0.32	0.26	0.40

Table 1. 3D accuracy evaluation w.r.t. in-situ measurements given in meters based on 26 reference points and two opposite orbit Staring Spotlight images.

Future work will deal with automatic transfer of those SAR-based GCPs to optical images by means of multi-modal image matching. Most promising recent works use deep learning to tackle this ill-posed issue, for instance, [7, 8, 1].

References

[1] T. Bürgmann, W. Koppe, and M. Schmitt. Matching of TerraSAR-X derived ground control points to optical image patches using deep learning. *ISPRS Journal of Photogrammetry and Remote Sensing*, 158:241–248, 2019.

[2] J. C. Curlander. Location of spaceborne SAR imagery. *IEEE Transactions on Geoscience and Remote Sensing*, (3):359–364, 1982.

[3] T. Fritz and M. Eineder. TerraSAR-X ground segment basic product specification document, TX-GS-DD-3302, issue 1.9. Technical report, DLR, 2013.

[4] S. Gernhardt, X. Cong, M. Eineder, S. Hinz, and R. Bamler. Geometrical fusion of multitrack PS point clouds. *IEEE Geoscience and Remote Sensing Letters*, 9(1):38–42, 2011.

[5] C. Gisinger, U. Balss, R. Pail, X. X. Zhu, S. Montazeri, S. Gernhardt, and M. Eineder. Precise three-dimensional stereo localization of corner reflectors and persistent scatterers with TerraSAR-X. *IEEE Transactions on Geoscience and Remote Sensing*, 53(4):1782–1802, 2014.

[6] S. S. Gleason, M. A. Hunt, and W. B. Jatko. Subpixel measurement of image features based on paraboloid surface fit. In *Machine Vision Systems Integration in Industry*, volume 1386, pages 135–144. International Society for Optics and Photonics, 1991.

[7] L. H. Hughes, M. Schmitt, L. Mou, Y. Wang, and X. X. Zhu. Identifying corresponding patches in SAR and optical images with a pseudo-siamese CNN. *IEEE Geoscience and Remote Sensing Letters*, 15(5):784–788, 2018.

[8] L. H. Hughes, M. Schmitt, and X. X. Zhu. Mining hard negative samples for SAR-optical image matching using generative adversarial networks. *Remote Sensing*, 10(10):1552, 2018.

[9] W. Koppe, R. Wenzel, S. Hennig, J. Janoth, P. Hummel, and H. Raggam. Quality assessment of TerraSAR-X derived ground control points. In *IEEE International Geoscience and Remote Sensing Symposium*, pages 3580–3583, 2012.

[10] F. W. Leberl. *Radargrammetric Image Processing*. Artech House, 1990.

[11] S. Montazeri, C. Gisinger, M. Eineder, and X. X. Zhu. Automatic detection and positioning of ground control points using TerraSAR-X multiaspect acquisitions. *IEEE Transactions on Geoscience and Remote Sensing*, 56(5):2613–2632, 2018.

[12] R. Perko. *Computer Vision for Large Format Digital Aerial Cameras*. PhD thesis, Graz, University of Technology, Austria, 2004.

[13] R. Perko, K. Gutjahr, M. Krüger, H. Raggam, and M. Schardt. DEM-based epipolar rectification for optimized radargrammetry. In *IEEE International Geoscience and Remote Sensing Symposium*, pages 969–972, 2017.

[14] R. Szeliski. *Computer Vision: Algorithms and Applications*. Springer Science & Business Media, 2010.